CHAPTER FOURTEEN

Space photovoltaics for extreme high-temperature missions

Geoffrey A. Landis
NASA John Glenn Research Center, Photovoltaic & Electrochemical Systems Branch, Cleveland, OH, United States

14.1 Introduction

Solar arrays for use on the surface of the Earth must be designed to withstand an extremely degrading environment: surrounded by a highly oxidizing atmosphere, intermittently exposed to corrosive liquid water, subject to wind loading, abrasion by sand and dust, and occasionally impacted by hail. Solar arrays for space are not subject to these effects, but instead have a different set of environmental hazards, including more extreme temperature cycles, particulate and ultraviolet radiation in space, micrometeoroid damage, and exposure to a flux of atomic oxygen in low-Earth orbit. Over the years since the first solar cells were sent into space on Vanguard 1 in 1958, space solar array technology has advanced to make photovoltaic cells resistant to these degradation mechanisms.

As each of the degradation mechanisms has been conquered, the range of environments in which we use photovoltaics has expanded outward [1], from initial use of arrays in low-Earth orbit, to satellites flying in the high-radiation environment of the Van Allen radiation belts, and outward to the dusty environment of Mars, the low-intensity (or illumination)/low-temperature (LILT) conditions in the asteroid belt and beyond, and with the success of the solar-powered Juno mission [2], even in the cold and high-radiation environment in Jupiter's orbit, with proposals made for photovoltaic power even farther beyond [3,4]. It is also, however, of interest to expand the range of solar arrays in the opposite direction: inward toward the Sun. The environment close to the Sun has its own unique challenges, with one of the most obvious being high temperatures.

Extending the temperature range of operation for solar arrays is highly desirable for extending the range of operation of space missions to the near-Sun environment [5–7]; interestingly, high temperatures help prevent arcing of solar arrays [8]. Achieving high-efficiency and reliable operation in these temperature regimes is a difficult technologic challenge. Existing solar cells lose performance at the high temperatures encountered in Mercury orbit and inward toward the Sun. For future missions designed

Photovoltaics for Space
ISBN 978-0-12-823300-9
https://doi.org/10.1016/B978-0-12-823300-9.00012-1

to probe environments close to the Sun, it is desirable to develop array technologies for high (light) intensity and high temperature (HIHT). Approaches to solar array design for near-Sun missions include thermal management at the systems level to optimize efficiency at elevated temperature or the use of techniques to reduce the incident solar energy to limit operating temperature. An additional problem is found in missions that involve a range of intensities, such as the Parker Solar Probe mission [9,10], which ranges from a starting distance of 1 astronomical unit (1 AU, roughly the distance from Earth to the Sun) from the Sun to a minimum distance of 9.5 solar radii, or 0.044 AU. During the mission, the solar intensity ranges from one to about 500 times the intensity at air mass zero (AM0). This requires a power system to operate over nearly three orders of magnitude of incident intensity. Another, more difficult problem is the environment of the surface of Venus [11]. In this case, the photovoltaics must operate at high temperature and low intensity, with the additional challenge of a modified spectrum shifted toward the red end of the spectrum [12] and a high-pressure, corrosive atmosphere.

14.2 Solar cell operating temperature and efficiency

If future missions designed to probe environments close to the Sun will be able to use photovoltaic power generation, solar cells that can function at high temperatures under high light intensity and high radiation conditions must be developed. The significant problem is that solar cells lose performance at high temperatures. In radiative equilibrium, the operating temperature of a solar cell depends on the fourth root of the incident intensity, as well as the ratio of solar absorptivity alpha (α) to thermal emissivity epsilon (ε). According to radiative balance, if I is the incident intensity, the thermal radiation from the array must equal the absorbed solar radiation:

$$\alpha \mathrm{I} = \left(\varepsilon_{\mathrm{f}} + \varepsilon_{\mathrm{r}}\right)\sigma \mathrm{T}^4 \tag{14.1}$$

where T is the operating temperature in absolute (Kelvin) units, and the subscripts f and r indicate the emissivity from the front and rear sides of the cell to account for the fact that the array can radiate waste heat away from both front and back sides (ε_{r} should be left out for an array with no backside radiation). For convenience, here we define the absorptivity α as the net energy absorption, incorporating a factor of $(1-\eta)$ to account for the fact that the fraction of incident energy that is converted to electricity is not radiated by the cell. Thus, the equilibrium operating temperature T is

$$\mathrm{T} = \left[\left(\alpha / \left(\left(\varepsilon_{\mathrm{f}} + \varepsilon_{\mathrm{r}}\right)\sigma\right)\right)\mathrm{I}\right]^{1/4} = \mathrm{c}\mathrm{I}^{1/4} \tag{14.2}$$

where the constant c is defined as

$$\mathrm{c} = \left[\alpha / \left(\left(\varepsilon_{\mathrm{f}} + \varepsilon_{\mathrm{r}}\right)\sigma\right)\right]^{1/4} \tag{14.3}$$

Note that since front and back sides of the cell need not have identical radiative properties in the infrared, the value of ε is the average of front and back side properties. The intensity depends on distance from the Sun:

$$I = I_o/r^2 \tag{14.4}$$

where I_o is the solar intensity at Earth's distance from the Sun, 1 AU, and distance r is measured in AU. This equilibrium temperature is shown as a function of distance from the Sun in Fig. 14.1 for various values of the ratio of the α to ε (here ε is the average of the front and back emissivity).

For the case of a planetary orbiter, the temperature is somewhat greater since the solar array is heated not only by the incident solar flux, but also by solar flux reflected by the planet (known as "albedo"), as well as infrared emitted by the planet. This additional heating becomes more significant as the orbital altitude decreases. In the lowest orbit limit, this results in about twice the incident intensity, so an absolute temperature increases by a factor of the fourth root of 2 ($\sim$1.19).

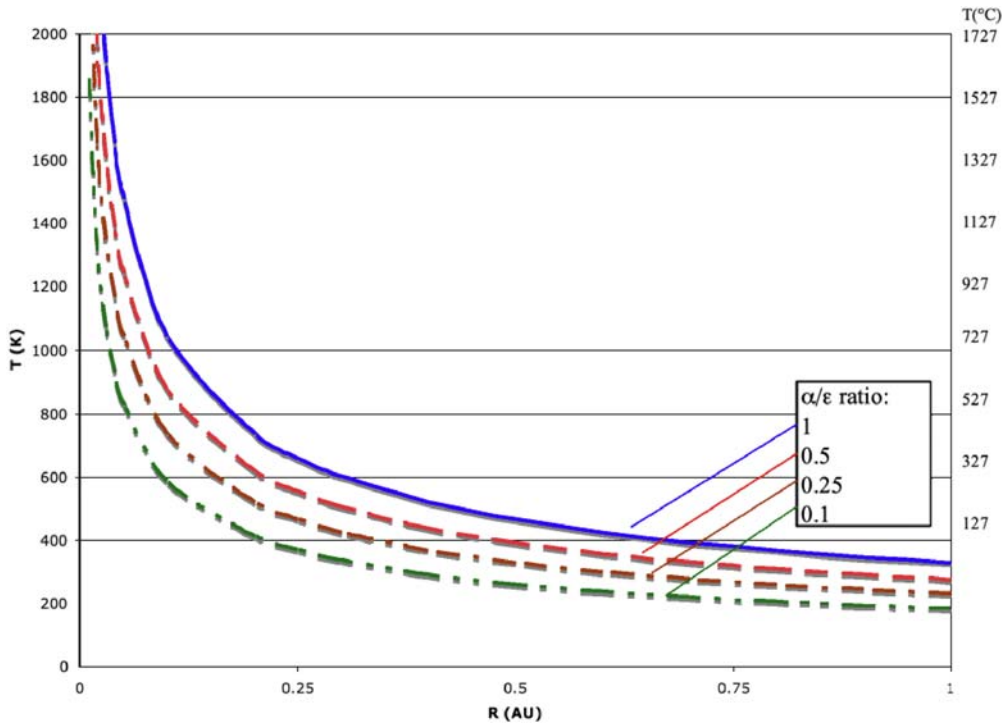

Figure 14.1 Temperature as a function of distance from the Sun, for various values of α/ε ratio. *Courtesy NASA.*

A solar cell's (unnormalized) temperature coefficient of efficiency κ is defined (Eq. 14.5) as the change of conversion efficiency η per unit temperature,

$$\kappa = d\eta/dT \tag{14.5}$$

and the power P at a temperature T can be compared to the power output from a reference temperature (Eq. 14.6), typically 27°C (300K) by a linear extrapolation:

$$P = (\eta_{300K} + \kappa\Delta T)I \tag{14.6}$$

In general, the temperature coefficient κ is negative, corresponding to decrease in performance with increasing temperature [13]. The temperature coefficient is not a constant but varies slightly with both intensity and temperature [14], discussed subsequently, but these variations for the moment can be ignored in a first-order analysis.

From this, the power output from a cell in radiative equilibrium is a nonlinear function of the intensity. Defining η_o as the efficiency linearly extrapolated to 0 K, which is calculated from the efficiency at 27°C as

$$\eta_o = \eta_{300K} - 300\kappa \tag{14.7}$$

Eq. (14.8) results:

$$P = I(\eta_o + \kappa T) = I\left(\eta_o + \kappa c I^{1/4}\right) = I\eta_o + \kappa c I^{5/4} \tag{14.8}$$

Fig. 14.2 shows the calculated curve of power output as a function of temperature, comparing a high-efficiency silicon solar cell with a wide-bandgap solar cell, in the case of the linear assumption. For any given solar cell technology, there exists an incident intensity above which the solar cell output decreases with increased intensity. In the linear model of Eq. (14.7), this intensity is as follows:

$$I_{peak-output} = (-\eta_o/\kappa c)^4 \tag{14.9}$$

14.3 Temperature coefficient(s)

Temperature coefficients of solar cells have been analyzed by Fan [13] and others [14,15]. The power output of a solar cell can be composed as the product of three factors, short-circuit current density (J_{sc}), the open-circuit voltage (V_{oc}), and the curve fill-factor (FF):

$$P = (J_{sc})(V_{oc})(FF) \tag{14.10}$$

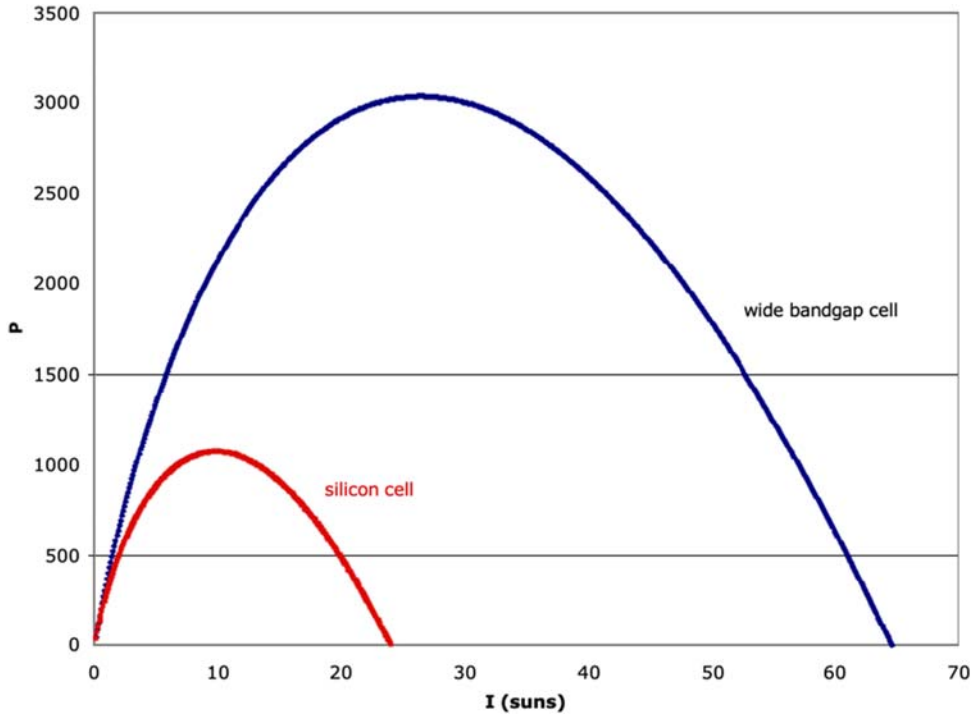

Figure 14.2 Curve of power output (normalized) as a function of intensity, assuming linear temperature coefficient. *Courtesy NASA.*

The variation of solar cell performance as a function of temperature can be approximated in terms of linear temperature coefficients:

$$J_{sc} = \frac{\mathrm{d}J_{sc}}{\mathrm{dT}}(\mathrm{T} - \mathrm{T_o}) \tag{14.11}$$

$$V_{oc} = \frac{\mathrm{d}V_{oc}}{\mathrm{dT}}(\mathrm{T} - \mathrm{T_o}) \tag{14.12}$$

$$\mathrm{FF} = \frac{\mathrm{dFF}}{\mathrm{dT}}(\mathrm{T} - \mathrm{T_o}) \tag{14.13}$$

where T is the temperature of interest, and $\mathrm{T_o}$ is the nominal test temperature (often set to 28°C).

Note that since these three factors all have different temperature dependence, the maximum power point voltage of a solar cell will also vary with temperature. For an

optimized system, the power management will need to account for this and adjust the operating point to maximize power if the spacecraft operates at a range of distances from the Sun. Alternately, the operating point voltage can be selected for the most power-critical phase of the mission, and losses associated with operation away from the maximum power point accepted for other phases of the mission, where power is less critical. Of the three components of temperature coefficient, voltage will decrease with increasing temperature, while short-circuit current will increase (due to bandgap narrowing). For well-optimized cells, the V_{oc} temperature coefficient contributes the largest amount to the total variation of efficiency with temperature.

Temperature coefficients are also often expressed in the form of normalized temperature coefficients, where the normalization is done by dividing by the value at T_o, so the variation is expressed as a fraction of the initial value. Using normalized temperature coefficients, the overall temperature coefficient will simply be the sum of the J_{sc}, V_{oc}, and FF components. The temperature coefficient is, in general, nonlinear. For this analysis we have been assuming a linear dependence of efficiency on temperature, but for a more detailed analysis, the nonlinearity must be accounted for in more detailed modeling.

Outside of a narrow temperature range, temperature coefficient for multijunction cells can be quite nonlinear. In particular, for multijunction cell technologies, the voltage component of the temperature coefficient is the sum of the voltage dependence of the individual subcells. At elevated temperature, the lowest bandgap subcells will drop to zero output, and beyond this point, the temperature coefficient will depend only on the remaining cells; this results in a discontinuous decrease in the temperature coefficient at higher temperature, as the lowest bandgap subcells in the series drop out. Likewise, since the bottom cells see a spectrum that has been filtered by the top cells in the cascade, and the bandgap of these top cells varies with temperature, the current component of the temperature coefficient can be nonlinear.

A temperature coefficient is also dependent on the illumination intensity [14–16]. The largest factor in temperature dependence is the dV_{oc}/dT term, which depends on the difference between the open circuit voltage of the cell and the bandgap voltage [6]. Since this decreases as the V_{oc} increases, κ decreases in magnitude proportionally to the V_{oc}, which increases as the logarithm of the intensity. This increases the output at high intensities slightly over the constant κ model.

The theoretical temperature coefficient of V_{oc} can found from the ideal solar cell equation (Eq. 14.14). As derived by Fan [13], for an ideal cell the temperature coefficient is as follows:

$$\frac{\partial V_{oc}}{\partial T} = \frac{1}{T}\left[V_{oc} - \frac{E_q}{q} - \frac{3kT}{q}\right] + \frac{1}{q}\frac{\partial E_q}{\partial T} + \frac{kT}{qJ_{sc}}\frac{\partial J_{sc}}{\partial T} \tag{14.14}$$

where T is temperature, E_g is the band gap energy in eV, k is Boltzmann's constant, and J_{sc} is the short-circuit current density of the solar cell. The factor q, electron charge,

converts the bandgap from units of electron-volts into units of volts. The first factor, in general, is large compared to the others, so we can usually ignore the second two factors. Thus, the temperature coefficient is proportional to the difference between the open circuit voltage V_{oc} and the bandgap E_g/q. V_{oc} is always less than the bandgap, so the temperature coefficient of V_{oc} is always negative.

The question of how to improve the temperature coefficient of solar cells has been addressed in earlier studies [5–7]. Since the fractional loss of V_{oc} with temperature decreases in magnitude as bandgap increases [13], photovoltaic cells from wide-bandgap materials can operate at higher intensity (so higher temperatures) than cells from narrow-bandgap materials [5–7]. Any advance that improves the open circuit voltage (to bring the voltage closer to the bandgap voltage) will also decrease the temperature coefficient.

For an array designed to operate at high temperature, it is also a requirement that the solar cell not physically degrade at high temperatures, for example, from degradation of the semiconductor or from ohmic contacts diffusing through the junction. Ohmic contacts that are stable at high operation temperatures have been demonstrated for GaAs [17–19] and $GaInP_2$ [20,21], but work remains to be done for other semiconductor

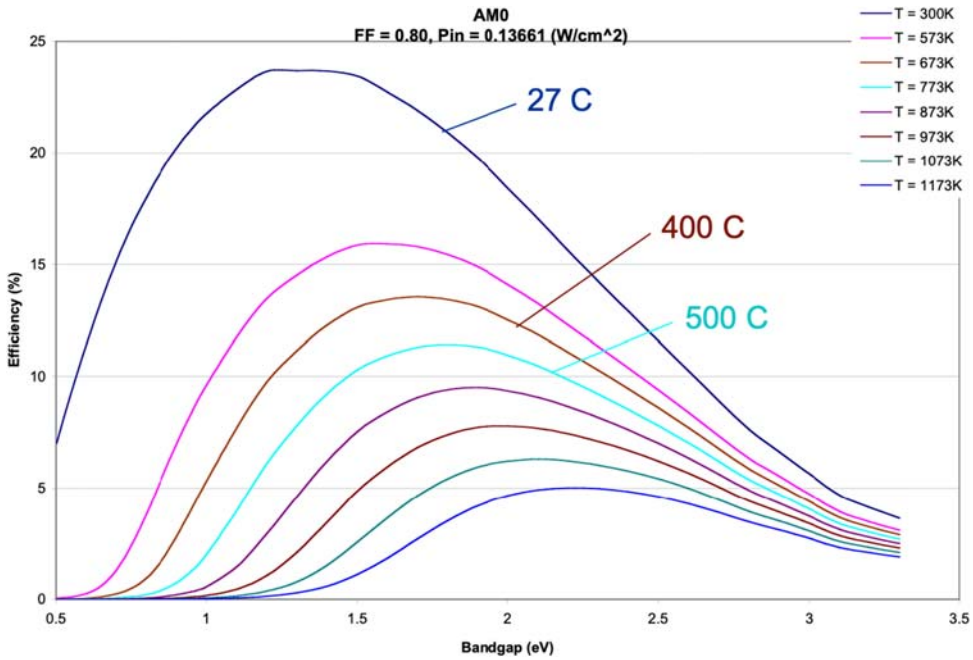

Figure 14.3 Modeled efficiency of a single-junction solar cell as a function of the semiconductor bandgap, for temperatures ranging from 27 to 900°C. *Courtesy NASA.*

technologies. Likewise, other components of the system, such as the cover glass adhesive and the interconnect, must be stable at high-temperature operation.

From the basic semiconductor diode calculation and the calculation of temperature coefficient as a function of bandgap, it is possible to calculate the effect of the solar cell bandgap on the efficiency as a function of temperature. Fig. 14.3 shows this calculation for a conventional single-junction cell. As is clear, the efficiency drops as the temperature increases. It is also notable that the optimum bandgap rises with increased operating temperature since higher bandgap solar cells have higher open circuit voltage, and thus lose a lower fraction of their voltage as the temperature increases.

14.4 Approaches to solar arrays for near-Sun missions

Approaches to solar arrays for near-Sun missions include modifying any of the terms governing temperature or efficiency of the cell: I, the incident intensity, α, solar absorption, or ε, the emissivity of the cell, or κ, the temperature coefficient. Possible approaches include the following:

1. high epsilon/low alpha coatings
2. array off-pointing (i.e., array normal points at angle to Sun)
3. partially populated array (with missing cells replaced with mirrors)
4. Spectrally selective reflective coatings
5. solar cells designed to operate at high temperature, with low temperature coefficient κ
6. solar arrays incorporating added thermal radiators

Since light that is not absorbed by the solar array does not contribute to the waste heat rejected by the radiator, it is advantageous to reflect light in the wavelengths not used by the cell. Most importantly, infrared light of energy less than the bandgap energy of the bottom subcell contains significant energy but makes no contribution to the output power. Blue-red rejection filters could enhance the performance of the radiators by reflecting this unused band. The three subcells of a multijunction cell contribute roughly equally to the temperature coefficient, although the bottom cell is only a small contributor to the overall efficiency. Thus, it is likely that even more heat rejection could be accomplished if the bottom (Ge) cell were omitted entirely from the stack, essentially returning the technologic approach toward the earlier dual-junction cell technology. This would allow all the energy of wavelength longer than about 850 nm to be reflected away by an infrared-rejection (dichroic) filter. Since the controlling parameter for the radiator sizing is the efficiency of conversion of the light absorbed by the cell, not the overall solar conversion efficiency, some reflection of the above-bandgap spectral range is acceptable, so the filter does not need a sharp cutoff at the band edge. This means that a thin metal film (for example, gold) or a transparent conductor could be a good choice for infrared rejection.

14.5 Solar arrays with constant power at variable heliocentric distance

An additional problem is presented in that most missions involve a range of intensities, requiring a power system capable of operating all the way from Earth departure through a close solar pass. There are several approaches to such a power system. One straightforward approach would be to utilize several different arrays, each one optimized for a different heliocentric distance. For example, a large solar array could be used for the highest solar distances, and then discarded, or else folded away in the shadow behind the spacecraft, so that a smaller solar array optimized for higher intensity could be used. Another approach would be to progressively use increasing amounts of off-pointing, so that the area exposed to the Sun decreases with distance. The problem of adapting to multiple intensity regimes is particularly difficult if the mission is required to operate both at a near-solar approach and also at distances farther from the Sun than the Earth, for example, missions using a gravity-assist at Jupiter, solar sail missions, and missions that follow a comet from distant reaches of the solar system through close approach to the Sun.

One approach is to design the array to produce a constant amount of power regardless of distance from the Sun. Fig. 14.4 shows a design that makes use of the fact that the angular diameter of the Sun increases as the spacecraft approaches the Sun. A Fresnel lens array focuses light onto a light pipe to transmits the light through a shield of multiple

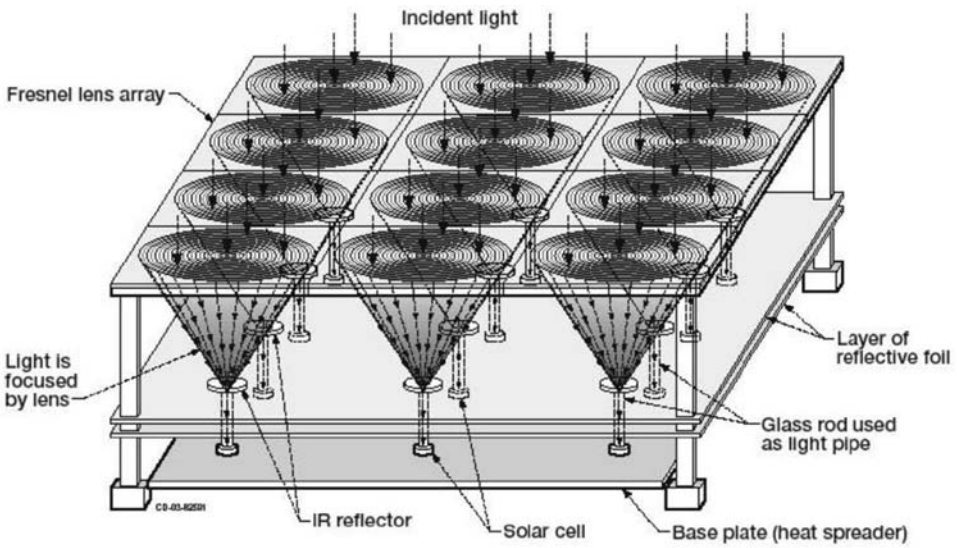

Figure 14.4 Concept for a concentrator solar array designed to have constant power output for variable heliocentric distances. *Courtesy NASA.*

layers of foil. At high distances from the Sun, the fact that the array is a concentrator array minimizes the effect of cell operation under LILT conditions. As the array approaches the Sun, the light pipe acts as an aperture stop. As the image of the solar disk at the focal plane gets larger, the added incident light is reflected by the mirrored plate. The solar cells are mounted on a heat spreader that allows the full backside surface to serve as a thermal radiator. The portions of the collector exposed to the sunlight are refractory material (silica or high-alumina glass for the optical elements; titanium or carbon for the structural components). The solar cells, located behind the multiple layers of metal-foil insulation, are not exposed to high temperature. This array can thus be designed to put an amount of solar intensity on the cells exactly equal to that of the peak defined above.

14.6 Thermal conversion for near-Sun missions

As a spacecraft approaches the Sun, the temperature of a flat plate exposed to the Sun increases. This brings out a natural question of whether it is possible to convert this heat, using a heat engine, rather than using photovoltaic arrays. Thermal power conversion is a demonstrated technology, and there exists a choice of conversion technologies, including thermoelectric conversion, a technology with comparatively low efficiency, but high spaceflight heritage, or Stirling conversion, which has the advantage of higher efficiency but no spaceflight heritage.

Stirling converters have demonstrated 38% conversion efficiency [22] operating at 850 hot-end, 90°C cold-end temperatures, which is slightly over 50% of the theoretical (Carnot) efficiency. System efficiency, accounting for other losses, is on the order of 26%. These efficiency numbers are roughly comparable to the best photovoltaic technologies. The efficiency scales with temperature directly with the Carnot efficiency, proportional to the difference between the hot- and cold-end temperature. Thermal conversion approaches would require a heat rejection radiator at the cold end of the system, which must be not exposed to the Sun, either in the shadow of an absorber or the thermal shield, or else edge-on to the incident flux. The radiator must be sized to radiate the waste energy at the cold-side temperature.

Fig. 14.5 shows the block diagram of the energy flow in such a thermal system. Since the power produced is proportional to the conversion efficiency η, and the radiator area proportional to the waste power radiated, which is proportional to $(1 - \eta)$, the radiator area A_r (Eq. 14.15), which depends sensitively on the conversion efficiency and the radiator temperature, is

$$A_r = [(1-\eta)/(\eta)]/\left(\varepsilon\sigma T^4\right) P_{electric} \tag{14.15}$$

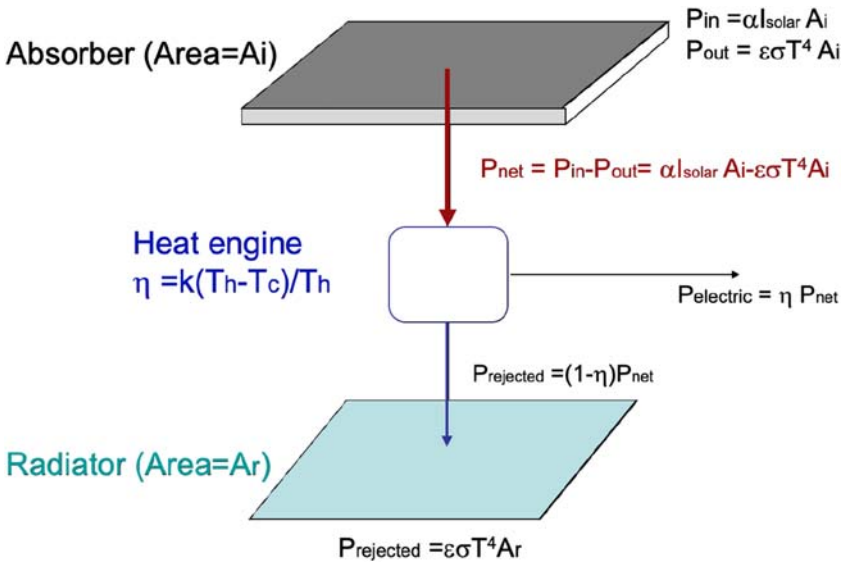

Figure 14.5 Thermal conversion energy flow block diagram. *Courtesy NASA.*

Emissivity ε for thermal radiators is typically very close to 1. If the radiator is two sided, the area A includes both front and rear sides. The same equation for radiator size can be used if the thermal radiator is used to cool a solar array instead of a heat engine.

The thermal system chosen must operate over a wide range of intensities, thus temperatures. This can represent an engineering challenge for many missions; for example, the Solar Probe is only at close approach to the Sun for a duration on the order of 10 h. The proposal to operate a thermal conversion system, incorporating a radiator with pumped cooling to achieve the cold-side temperature, brings up the possibility of using a similar cooling loop to keep a solar array within operating temperature limits, thus reducing the requirement for high-temperature operation. This approach was adopted for the Parker Solar Probe (Section 14.8).

14.7 Earlier near-Sun missions

Early missions to operate in a near-Sun environment include the Soviet Venera missions and the US Mariner 10 mission to Venus and Mercury. More recently, the solar-powered Mercury Surface, Space Environment, Geochemistry and Ranging (MESSENGER) mission successfully reached and orbited Mercury, and the ESA BepiColumbo mission is on its way to Mercury. Due to the high temperatures to be experienced, starting with spacecraft Venera 2 and Venera 3, launched in November 1965, the Soviet Venus missions utilized gallium arsenide solar cells [23], despite the fact that GaAs-based cells were at a lower state of development in the 1960s and would not supplant silicon cells for conventional space missions until the very end of the 1980s.

Figure 14.6 Solar panel for the MESSENGER mission, showing that two-thirds of the array area is covered with mirrors, and only one-third of the area (dark stripes in the image) has solar cells. *Courtesy NASA.*

The reason for their choice was that the wider bandgap of GaAs (1.4 eV, compared to silicon at 1.1) gave it a significantly lower temperature coefficient, so better performance at Venus. The Mariner series took a different approach. The Mariner 10 spacecraft kept the (at the time) industry-standard silicon cell technology, but it employed the technique of gimbaling the solar arrays away from the Sun-pointing direction to minimize the temperature [1]. This reduces the incident solar flux by a factor of cos(ø), where ø is the off-pointing angle, so it reduces the temperature by a factor of $\cos^{(1/4)}$ (ø).

As an example of a mission with solar panels designed to operate at high solar flux using both limiting the incident flux to the array and modifying solar absorption (α), the MESSENGER mission to orbit Mercury [24,25] had designed an array with mirrored panels (Fig. 14.6) to reflect two-thirds of the incident solar energy to limit operating temperature. The mirrors incorporate a high-emissivity silica coating, allowing efficient thermal radiation [26]. In addition to the reflectors, the MESSENGER arrays also used off-pointing to fold the solar arrays back along the spacecraft body to reduce the incident flux. These panels were successfully operated during the full 10.5 year mission, including the cruise to Mercury and for over 4 years in Mercury orbit. The mission reached a minimum distance of 0.3 AU from the Sun, and the arrays had been qualified in thermal vacuum testing to be capable of operating as close as 0.25 AU from the Sun, at an intensity of 16 times the intensity at Earth orbit. Likewise, the BepiColumbo spacecraft utilizes a strategy to tilt its solar arrays off the Sun-pointing axis to reduce the incident solar flux to keep the temperature within limits, up to an angle of over 70 degrees at a distance of 0.3 AU [27].

14.8 Parker Solar Probe

The highest solar intensity encountered by a mission flown to date is that seen by the Parker Solar Probe. The mission concept for the Solar Probe mission incorporated

multiple Venus flybys to drop the probe into a low-perihelion orbit. The primary mission uses seven Venus flybys to bring its orbit incrementally closer to the Sun, making 24 near-Sun passes over a period of 6.9 years, with a final objective of reaching a perihelion distance of roughly 9.6 solar radii, or 0.044 AU, significantly inside the orbit of Mercury. This will be about eight times closer than any spacecraft has previously approached the Sun.

An enabling technology for the mission was to design a power system that could not only operate at the highest intensity portion of the mission, at and near the perihelion pass close to the Sun, but also provide power during the cruise and multiple Venus flybys. The array design therefore had to provide power at all distances from 1 AU down to 0.044 AU [9]. A solar array strategy was designed to meet these criteria [10]. The strategy adopted was to use two solar arrays:

1. *Conventional solar array*: The primary array is used from Earth to slightly inside the Mercury orbit. Since the MESSENGER array is already demonstrated in flight, the engineering assessment concluded that only a small amount of cell and materials development is needed. The array can be off-pointed from the Sun by progressively folding them back along the spacecraft body, to allow operation in to approximately 0.25 AU, an intensity of 16 suns. At this distance the main solar array is folded in behind the shadow shield, where it is not exposed to high temperatures, and a second power supply is used.
2. *High-intensity solar array:* A secondary solar array (Fig. 14.7) was then incorporated to power the mission at the high-intensity portion of the mission, operating inside 0.25 AU. Since at this distance the intensity was high, the secondary solar array could be much smaller. This power supply used high-efficiency triple-junction solar cells

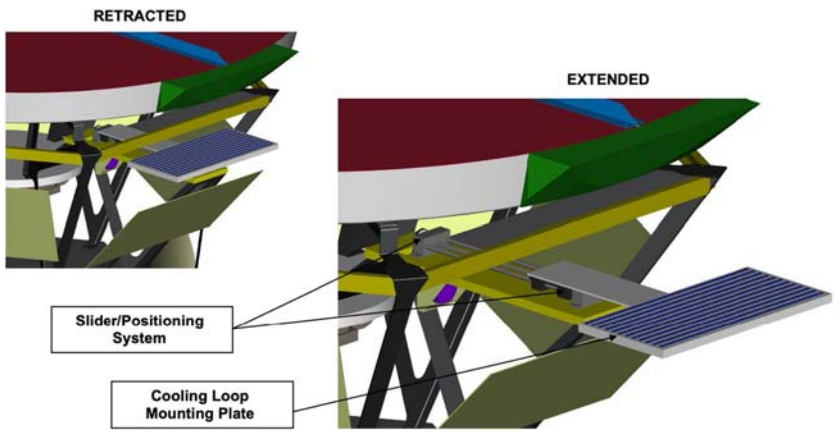

Figure 14.7 The early concept for the secondary (high-intensity) solar array for the Solar Probe+ mission, designed to be retracted behind a knife-edge shadow shield as the spacecraft approaches the closest distance from the Sun. *Courtesy NASA.*

designed for high solar concentrations. To keep the solar cells within the nominal temperature limits as the solar intensity increased, a liquid cooling loop was incorporated to pump coolants through thermal radiators mounted behind the solar shade on the outside of the spacecraft.

At the closest approach to the Sun, the secondary array was progressively slid behind a knife-edge shadow shield, moving the array into a partial shadow (penumbra). This was done both to keep the array power constant as the solar intensity increased and also as a way to reduce the thermal load that needed to be sent to the radiators. Details of the solar array design process are provided by Landis et al. [10]. This power system design solved the spacecraft's problems; it was presented to the review board, who approved the mission to go forward.

The final spacecraft design, now renamed Parker Solar Probe, differed from the initial design in several ways, although keeping the concept of a main solar array for operation near aphelion and a smaller high-intensity array for operation near perihelion. The secondary high-intensity solar arrays were relocated from their original position to put them at the end of the primary solar arrays, although set at an angle to the primary arrays. In this new position, the sliding mechanism was now unnecessary, and the rotation that angled the primary arrays back now also served as the mechanism to move the secondary arrays. At close distances to the Sun, the primary arrays are folded back behind the shadow shield, leaving only the secondary arrays, at the tip, exposed. As the spacecraft approaches yet closer to the Sun, additional angling slides (and rotates) the secondary arrays behind the knife-edge that progressively puts them in partial shadow from the full

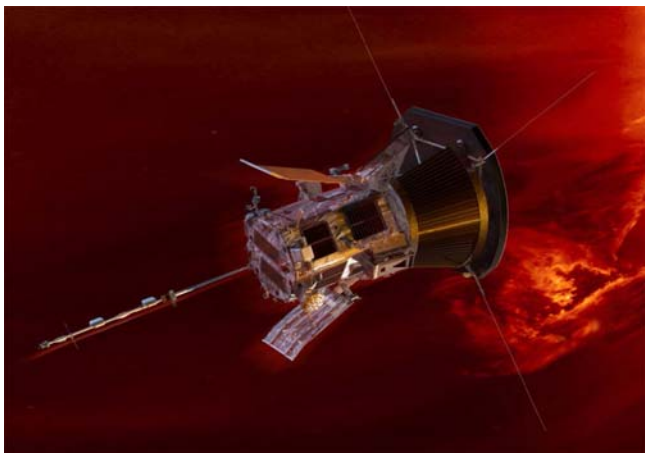

Figure 14.8 Artist's conception of Parker Solar Probe approaching the Sun, with main solar arrays feathered back. This spacecraft is designed to be operated on photovoltaic power as close as 0.044 AU from the Sun. The flat solar shield protects the instrument package from the thermal environment near the Sun. *Courtesy: NASA/Johns Hopkins APL/Steve Gribben.*

intensity of the solar flux. The net result incorporates the functionality but is mechanically much simpler than the initial concept.

An artist's conception of the revised design can be seen in Fig. 14.8, where the conventional arrays are shown feathered backward behind the shadow shield, protecting them from the peak solar intensity, and the secondary arrays, located at the tips of the primary arrays, are angled slightly to view the Sun. A second improvement to the design was in the coolant loop. In the revised design, the coolant loop is not just circulated behind the high-intensity panel, but it is also circulates behind the main solar array. This serves three functions: during the perihelion approach to the Sun, the area of the main array serves as additional radiator area; during the solar approach portion of the mission, before (and after) the nearest passage, the cooling reduces the load on the solar array; and during the portion far from the Sun, the solar input to the main array actually serves to keep the cooling liquid from freezing.

Gaddy et al. provide details of the Solar Probe mission arrays [28]; solar power output calculations are described in a subsequent publication [29]. The mission, now renamed Parker Solar Probe in honor of physicist Eugene Parker (1927–2022), who predicted the existence of the solar wind, launched in 2018. As of early 2022, it has successfully made five Venus flybys and 11 perihelion passes close to the Sun, with the power system operating perfectly.

14.9 Photovoltaic power at Venus

The surface of Venus is a target of great interest to science, but it is the most hostile operating environment of any of the solid-surface planets in the solar system [30]. The surface of Venus has been explored by a number of missions from Earth, including the Russian Venera missions that landed probes on the surface and the American Pioneer missions that flew both orbiters and atmospheric probes to Venus, but the longest survival time of any mission to the surface of Venus, to date, has been only 2 hours on the surface of Venus [11]. Four effects make the surface of Venus a challenging environment when considering solar power [12]:

(1) temperature
(2) solar intensity
(3) solar spectrum
(4) corrosive environment

The greatest difficulty is the surface temperature of Venus, averaging 452°C, with little difference between daytime and nighttime. As on Earth, temperature decreases with elevation, and the tops of Venus' mountains are slightly cooler: at the top of Maxwell Montes (10.4 km above mean elevation), the temperature is "only" 390°C. Secondarily, Venus is continually covered with a thick layer of clouds. The surface does not ever get a direct view of the Sun, and the solar intensity at the surface is about 2% of the intensity above the atmosphere. The light level is equivalent to the light level during a rainy day on Earth. The thick atmosphere also filters the sunlight, with the surface solar spectrum

depleted in blue wavelengths due to Rayleigh scattering. The surface pressure is 92 bars, equivalent to pressure a kilometer under the ocean, and the atmosphere is primarily of carbon dioxide. The atmosphere at the surface also contains significant amounts of anhydrous sulfur compounds, such as SO_3, which are corrosive. At the temperatures and pressures of the surface, stability against chemical attack is a significant concern.

These factors combine to multiply the challenges of power on the surface. The low light intensity alone reduces power availability, and the reduction of performance of solar cells due to temperature exacerbates this difficulty. This puts the solar cell operation into the low-intensity, high-temperature (LIHT) regime [31], a somewhat different regime from the HIHT region discussed previously.

For high-temperature operation, as discussed before, a high-bandgap solar cell material would be preferred, but the blue-deficient spectrum puts a limit on the availability of short-wavelength photons. Nevertheless, an analysis by Landis and Haag [12] showed that photovoltaic power systems, although limited in power, could produce power on the surface. Further work by Grandidier et al. [20,31] extended this work and tested cells to verify performance at Venus temperatures. Their lifetime testing showed degradation beginning at about 7 weeks of exposure at 465°C [31].

The problem of encapsulation of cells to protect against the corrosive effects of the Venus atmosphere, however, has yet to be addressed. While the glass used for solar cell covers is unaffected by the atmosphere or the temperature, preliminary testing under Venus conditions has shown that conventional silicone adhesives used to adhere cover glass to solar cells will blacken under Venus conditions. A possible solution would be direct bonding of a thermal expansion coefficient-matched glass to the cell, taking care that the bonding must be completely sealed, since even small amounts of leakage would be likely to corrode the cell, the metallization, and the electrical interconnects.

14.10 Conclusions

Operation of photovoltaic arrays at the high solar intensity conditions of near-Sun missions presents unique challenges to solar cell technology. If the temperature of an array is allowed to vary with the thermal radiation limit, the power produced by an array will increase as the incident flux increases up to some limit determined by the temperature coefficient and thermal properties of the solar cell, and above that output, power will decrease as incident intensity increases. A number of approaches have been developed to mitigate the effects of high-temperature operation. Several of these have been successfully demonstrated to enable solar-powered spacecraft to explore the near-Sun planets such as Mercury and Venus as well as the Sun itself.

References

[1] C.R. Mercer, Solar array designs for deep-space science missions, in: S.G. Bailey, A.F. Hepp, D.C. Ferguson, R.P. Raffaelle, S.M. Durbin (Eds.), Photovoltaics for Space: Key Issues, Missions and Alternative Technologies, Elsevier, 2022, pp. 349–378.

[2] S. Dawson, P. Stella, W. McAlpine, G. Smith, in: JUNO Photovoltaic Power at Jupiter, in: 10th International Energy Conversion Engineering Conference, 30 July–1 August 2012, Atlanta, GA, USA, https://doi.org/10.2514/6.2012-3833.

[3] A. Boca, R. Warwick, B. White, R. Ewell, A data-driven evaluation of the viability of solar arrays at Saturn, IEEE J. Photovoltaics 7 (4) (2017) 1159–1164.

[4] G.A. Landis, J. Fincannon, Study of power options for Jupiter and outer planet missions, in: Proc. 42nd IEEE Photovoltaic Specialists Conference, New Orleans LA, June 14–19, 2015, https://doi.org/10.1109/PVSC.2015.7356136.

[5] D. Merritt, S. Houlihan, R. Raffaelle, G. Landis, Wide bandgap space solar cell development, in: Proc. 21st. IEEE Photovoltaic Specialist's Conference, 2005, pp. 552–555.

[6] G.A. Landis, P. Jenkins, D. Scheiman, R. Raffaelle, Paper AIAA-2004-5578, Extended temperature solar cell technology development, in: Proc. 2nd International Energy Conversion Engineering Conference, August 16–19, 2004, Providence, RI, USA, https://doi.org/10.2514/6.2004-5578.

[7] G.A. Landis, R. Raffaelle, D. Merritt, High temperature solar cell development, in: Proc. 19th European Photovoltaic Science & Engineering Conference, 2004, pp. 3659–3661.

[8] D.C. Ferguson, New frontiers in spacecraft charging, IEEE Trans. Plasma Sci. 40 (2) (February 2012) 139–143, https://doi.org/10.1109/TPS.2011.2172635.

[9] J.D. Kinnison, A.A. Dantzler, Y. Guo, S. Vemon, C. DeBoy, M.M. Donegan, D. Drewry, et al., The Solar Probe+ Mission: a new concept for close solar encounters, in: Proc. 59th International Astronautical Congress, Glasgow, Scotland, Sept. 29–Oct. 3, 2008, vol 3, IAC, 2008, pp. 1596–1604.

[10] G.A. Landis, P.C. Schmitz, J. Kinnison, M. Fraeman, L. Roufberg, S. Vernon, M. Wirzburger, Power system design for the solar Probe+ mission, in: 6th International Energy Conversion Engineering Conference, Cleveland, OH, USA, July 28–30, 2008, https://doi.org/10.2514/6.2008-5712.

[11] G.A. Landis, Power systems for Venus missions: a review, Acta Astronaut. 187 (Oct. 2021) 492–497.

[12] G.A. Landis, E. Haag, Analysis of solar cell efficiency for Venus atmosphere and surface missions, in: AIAA 11th International Energy Conversion Engineering Conference, San Jose, CA, USA, July 15–17, 2013. Available at: https://doi.org/10.2514/6.2013-4028.

[13] J.C.C. Fan, Theoretical temperature dependence of solar cell parameters, Sol. Cells 17 (1986) 309–315.

[14] M.Y. Feteha, G.M. Eldallal, The effects of temperature and light concentration on the GaInP/GaAs multijunction solar cell's performance, Renew. Energy 28 (2003) 1097–1104.

[15] M.A. Green, General temperature dependence of solar cell performance and implications for device modelling, Prog. Photovoltaics 11 (5) (August 2003) 333–340.

[16] G.A. Landis, D.J. Belgiovane, D.A. Scheiman, Temperature coefficient of multijunction space solar cells as a function of concentration, in: Proc. 37th IEEE Photovoltaic Specialists Conference, Seattle WA, June 19–24, PVSC, 2011, pp. 1583–1588.

[17] S.P. Tobin, M.B. Spitzer, C. Bajgar, L. Geoffroy, C.J. Keavney, Advanced metallization for highly efficient solar cells, in: Proc. 19th IEEE Photovoltaic Specialists Conference, 1987, pp. 70–75.

[18] M. B Spitzer, J.E. Dingle, R.P. Gale, P. Zavracky, M. Boden, D.H. Doyle, Gallium arsenide concentrator solar cells with highly stable metallization, in: Proc. 20th IEEE Photovoltaic Specialists Conference, 1988, pp. 930–933, https://doi.org/10.1109/PVSC.1988.105840.

[19] M.B. Spitzer, J.E. Dingle, High Temperature Metallization System for Contacting Semiconductor Materials, U.S. Patent 5,075,763 (Dec. 24, 1991).

[20] E.E. Perl, J.S.D.J. Friedman, N. Jain, P. Sharps, C. McPheeters, Y.S.M.L. Lee, M.A. Steiner, (Al) GaInP/GaAs tandem solar cells for power conversion at elevated temperature and high concentration, IEEE J. Photovoltaics 8 (2) (2018) 640–645.

[21] J. Grandidier, A.P. Kirk, P. Jahelka, M.A. Stevens, P.K. Gogna, D. Crisp, M.L. Osowski, T.E. Vandervelde, H.A. Atwater, J.A. Cutts, Photovoltaic operation in the lower atmosphere and at the surface of Venus, Prog. Photovoltaics Res. Appl. 28 (6) (June 2020) 545–553, https://doi.org/10.1002/pip.3214.
[22] J. Chan, J. Wood, J. Schreiber, Development of advanced Stirling radioisotope generator for space exploration, in: Space Technology and Applications International Forum Conference, 2007. NASA/TM-2007-214806.
[23] V.M. Andreev, GaAs and high-efficiency space cells, in: Chapter ID-1, Practical Handbook of Photovoltaics, second ed., Academic Press, 2012, pp. 399–416.
[24] A.G. Santo, R.E. Gold, R.L. McNutt Jr., S.C. Solomon, C.J. Ercol, R.W. Farquhar, T.J. Hartka, et al., The MESSENGER mission to Mercury: Spacecraft and mission design, Planet. Space Sci. 49 (14–15) (December 2001) 1481–1500.
[25] J. McAdams, R.W. Farquhar, A.H. Taylor, B.G. Williams, MESSENGER mission design and navigation, Space Sci. Rev. 131 (1–4) (August 2007) 219–246, https://doi.org/10.1007/s11214-007-9162-x.
[26] G. Dakermanji, J. Jenkins, C.J. Ercol, The MESSENGER spacecraft solar array design and early mission performance, in: Proc. 2006 IEEE 4th World Conference on Photovoltaic Energy Conversion, vol 2, 2006, pp. 1919–1922.
[27] C.G. Zimmermann, C. Nömayr, M. Kolb, A. Caon, A solar cell design for the bepi Colombo high intensity—high temperature mission, in: 37th IEEE Photovoltaic Specialists Conference, 2011, pp. 3713–3718.
[28] E. Gaddy, R. Decker, M.K. Lockwood, L. Roufberg, G. Knutzen, D. Marsh, The Solar Probe Plus solar array development and design, in: Proc. 35th IEEE Photovoltaic Specialist's Conference, Honolulu, HI June 20–25, 2010, 2010, pp. 717–722, https://doi.org/10.1109/PVSC.2010.5617077.
[29] E. Gaddy, M. Butler, M.K. Lockwood, G. Martin, L. Roufberg, C. Vigil, A. Boca, B. Richards, R. Stall, M. Schurman, Predicting the solar probe plus solar array output, in: Proc. 40th IEEE Photovoltaic Specialist Conference, Denver CO, June 8–13, 2014, 2014, pp. 2155–2160, https://doi.org/10.1109/PVSC.2014.6925352.
[30] A. Bermudez-Garcia, P. Voarino, Olivier Raccurt, Environments, needs and opportunities for future space photovoltaic power generation: A review, Appl. Energy 290 (2021) 116757.
[31] J. Grandidier, A.P. Kirk, M.L. Osowski, P.K. Gogna, S. Fan, M.L. Lee, M.A. Stevens, et al., Low-intensity high-temperature (LIHT) solar cells for Venus atmosphere, IEEE J. Photovoltaics 8 (6) (2018) 1621–1626.